PAPER

Check for updates

Iridium (Ir) and osmium (Os) modified BP/BSe heterostructures as promising nanoscale molecule sensors for detection of H_2S, SO_2F_2 and SOF_4 gases: a DFT outlook

Amirali Abbasi (ID) *

A density functional theory approach was utilized to gain insights into the electronic properties and optimized structures of the novel Ir and Os modified BP/BSe heterostructures as gas sensing substrates for the detection of H_2S, SO_2F_2 and SOF_4 molecules. The band gap of 1.20 eV represents the excellent semiconducting properties of the BP/BSe heterostructure. The formation energies for the most stable structures of Ir and Os modified BP/BSe systems were calculated to be −3.17 eV and −1.92 eV, respectively, indicating the significant geometric stability of the studied heterostructures. The optimized Ir−Se and Os−Se bond lengths were measured to be 2.51 Å and 2.46 Å, respectively. The considered H_2S, SO_2F_2 and SOF_4 molecules were strongly chemisorbed on the Ir modified BP/BSe heterostructures. The highest adsorption energy of −2.97 eV was observed for SO_2F_2 molecules, which show dissociative adsorption with S−F bond cleavage. The newly formed Ir−F bond lengths were calculated to be 1.98 Å. The important objective of this research is to design an innovative BP/BSe heterostructure based sensor device for the detection of H_2S, SO_2F_2 and SOF_4 molecules.

1. Introduction

The increasing concentrations of environmental pollutants and gas emissions from industrial activities and different technologies have raised significant concerns about human life. To ensure the security and safety of human life and prevent environmental issues, toxic gas monitoring should be effectively performed. Researchers have consistently worked on new sensing nanomaterials in response to the increasing demand for highly efficient and appropriate gas sensors.[1–5] In recent decades, two-dimensional (2D) nanomaterials with high electrical conductivity and extensive surface area, have shown significant potential in the field of detecting and trapping harmful gas molecules.[6–8]

The promising applicability of 2D substrates such as antimonene and arsenene for detection of hazardous gases has attracted scientific research interest. Some theoretical studies have been devoted to investigating the incorporation of different transition metal and non-metallic elements into 2D nanosheets to improve the adsorption performance for detecting NO and CO gases.[9–11] Experimental studies have revealed that transition metals and non-metallic elements used for the modification of nanomaterial structures can effectively enhance gas adsorption efficiency. Given the growing demand for gas

sensing devices, there is a crucial need to fabricate and design novel sensing systems.

In recent years, significant studies have been devoted to exploring the properties of different nanomaterials for their potential in harmful gas sensing. These nanomaterials include 2D nanosheets, carbon based materials, boron nitrides, transition metal dichalcogenides and metal nanoclusters.[12–19] The emergence of novel nanomaterials with outstanding physical and chemical characteristics has recently triggered substantial interest in their application in sensor platforms, due to their outstanding abilities in adsorption and catalytic processes. In this regard, van der Waals heterostructure systems composed of 2D nanosheets pave the way for the fabrication of efficient systems for various applications such as gas sensors or electronic devices.[20,21]

Furthermore, modification of the surface of heterostructures has been considered as a promising strategy to enhance activity and modify the adsorption and electronic properties. Recent investigations have greatly highlighted the favorable properties of heterostructure systems. These hybrid structures are known for their excellent characteristics in comparison with the pristine monolayers while combining the properties of monolayers. Thus, the exploration of novel heterostructure materials can offer an important approach for constructing novel functional nanomaterials for various applications.[22–25] Meng *et al.* explored the properties of novel GaN/PtSe2 van der Waals heterostructures and demonstrated their strong potential in

Department of Chemistry Education, Farhangian University, P.O. Box 14665-889, Tehran, Iran. E-mail: abbasi.phchemist@gmail.com

photocatalysis.[26] It has been widely reported that the surface properties of nanomaterials can be drastically enhanced by doping and adsorption of transition metals and gas molecules.[27–30] Bo *et al.*[31] explored the detection of harmful gases like NO_2 and NO using superior sensor systems based on GaN–MoSSe heterostructures functionalized with Cu, Fe and Mn transition metals.

In this research, we modeled a suitable heterostructure system using monolayers of BP and BSe nanomaterials and investigated their stability and electronic properties using first principles calculations. After the decoration of BP/BSe heterostructures with Ir and Os transition metals, the adsorption properties of gases including H_2S, SO_2F_2 and SOF_4 molecules on these heterostructures were explored. The electronic band structures, charge density differences, work functions, density of states and recovery times were examined for the adsorption systems. These findings suggest that iridium and osmium

modified BP/BSe heterostructures show unique effectiveness for application in detecting harmful gases.

2. Methods and calculation models

All the density functional theory calculations[32,33] and simulations in this research were performed using the SIESTA package.[34,35] Double-zeta polarized (DZP) basis sets were considered for predicting the optimized geometries and electronic properties. The generalized gradient approximation (GGA) with the Perdew–Burke–Ernzerhof functional was applied to the systems for all structural optimization and energy calculations.[35] The GDIS program was also utilized to construct the structure of hybrid systems and manipulate the final structures.[36] Monkhorst–Pack K points of $8 \times 8 \times 1$ were applied in the calculations.[37] The van der Waals (vdW) interaction between the heterostructures and the gas molecules is described based on the DFT-D2 method of Grimm.[38]
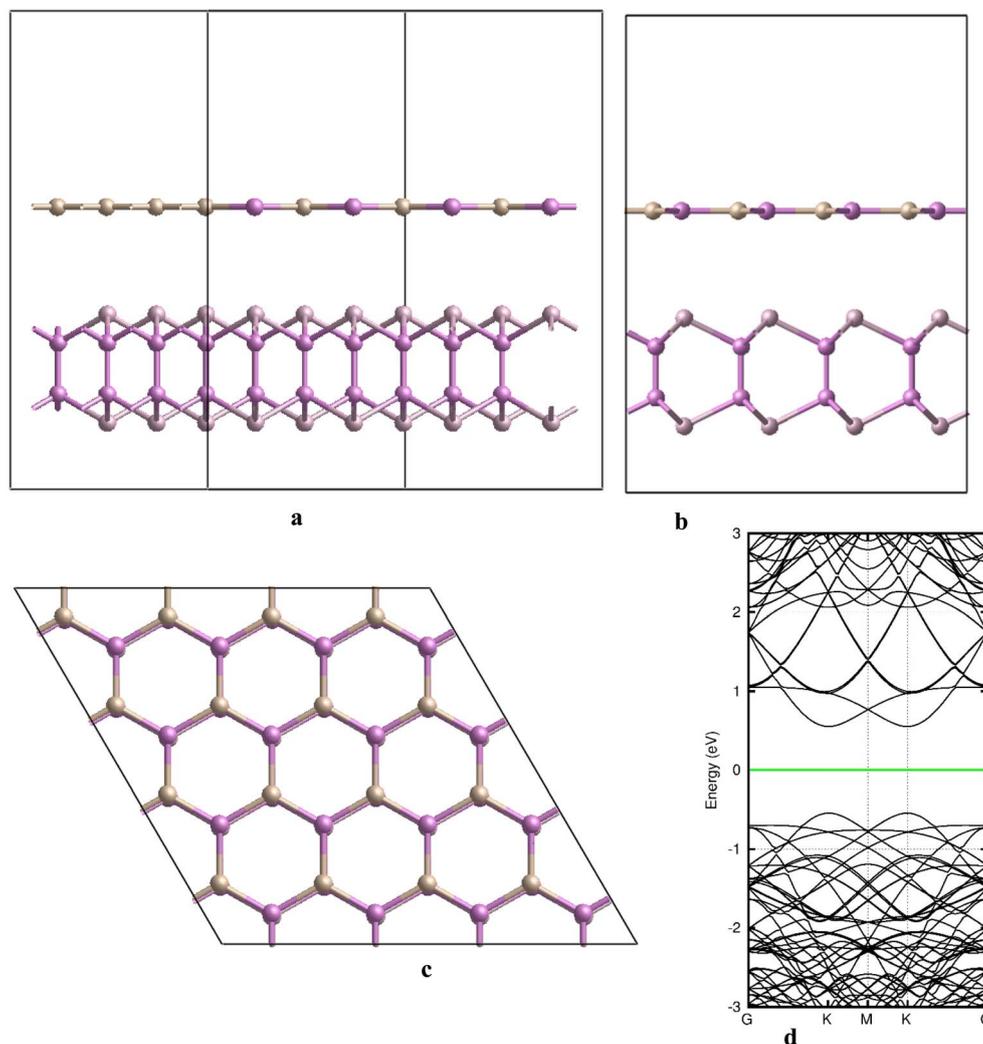

Fig. 1 Optimized structure of the heterostructure compound composed of a BP monolayer stacked with a BSe monolayer in three different views (a–c) and the corresponding energy band structure (d).
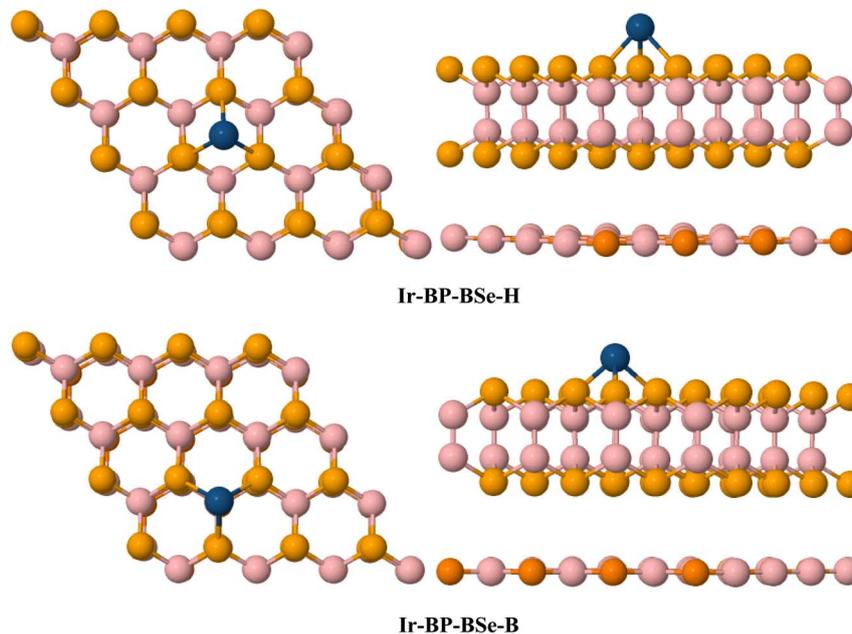
Ir-BP-BSe-H

Ir-BP-BSe-B

Fig. 2 Optimized structures of the Ir modified BP/BSe heterostructure systems.

Table 1 Formation energies and distances for Ir- and Os-modified BP/BSe heterostructures

Stacking model	Formation energy (eV)	Distance (Å)
Ir-BP-BSe-H	−3.17	2.51 (Ir–Se)
Ir-BP-BSe-B	−2.80	2.48 (Ir–Se)
Os-BP-BSe-H	−1.92	2.46 (Os–Se)
Os-BP-BSe-B	−1.76	2.39 (Os–Se)

The strength of interaction between the considered gases and the Ir-modified BP/BSe heterostructures was evaluated using the adsorption energy (E_{ads}) according to the following equation:

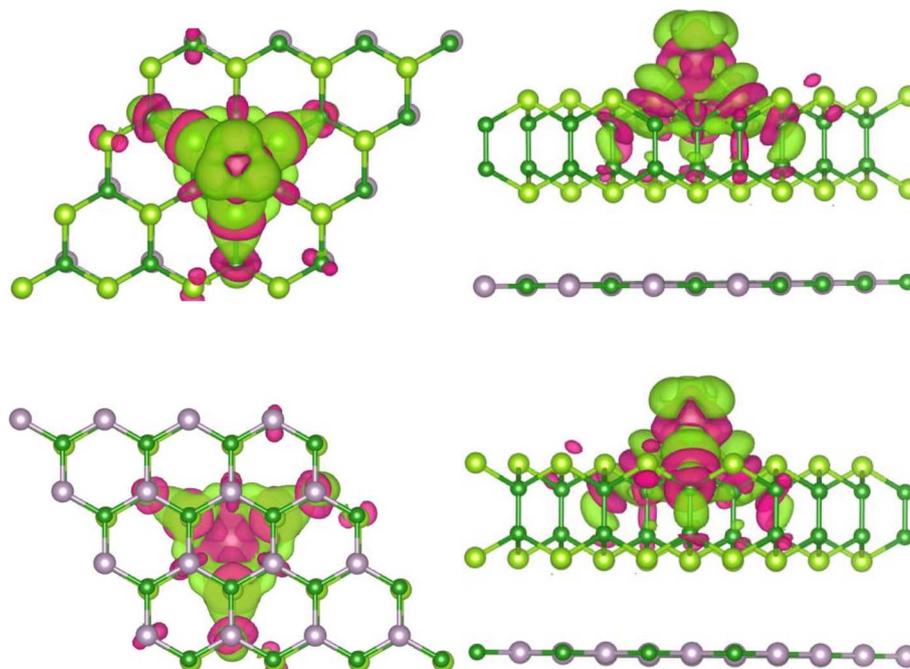$$E_{ads} = E_{Ir-BP/BSe-Molecule} - (E_{Ir-BP/BSe} + E_{Molecule}) \qquad (1)$$

Fig. 3 CDD diagrams of the Ir modified BP/BSe heterostructure systems with violet and green colors representing charge accumulation and depletion, respectively.

where E_{Molecule}, $E_{\text{Ir-BP/BSe}}$, and $E_{\text{Ir-BP/BSe-Molecule}}$ denote the energies of the gas molecules, the Ir modified BP/BSe vdW heterostructure, and the gas/Ir-BP/BSe hybrid system, respectively.

3.   Results and discussion

3.1   Ir and Os modified BP/BSe heterostructures

Before substantiating the electronic properties and structures of the Ir and Os modified BP/BSe heterostructures, the structure of
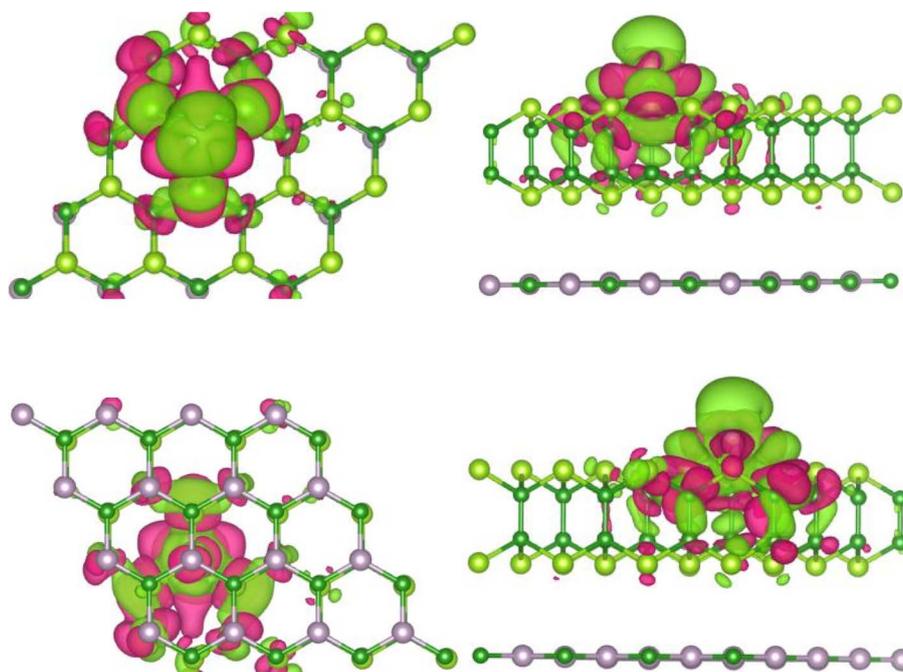

Fig. 4   CDD diagrams of the Ir modified BP/BSe heterostructure systems with violet and green colors representing charge accumulation and depletion, respectively.

Fig. 5   Band structure diagrams of the Ir modified BP/BSe heterostructure systems.

© 2025 The Author(s). Published by the Royal Society of Chemistry

Os-BP-BSe-H

Os-BP-BSe-B

Fig. 6 Optimized structures of the Os modified BP/BSe heterostructure systems.

Fig. 7 CDD diagrams of the Os modified BP/BSe heterostructure systems with violet and green colors representing charge accumulation and depletion, respectively.
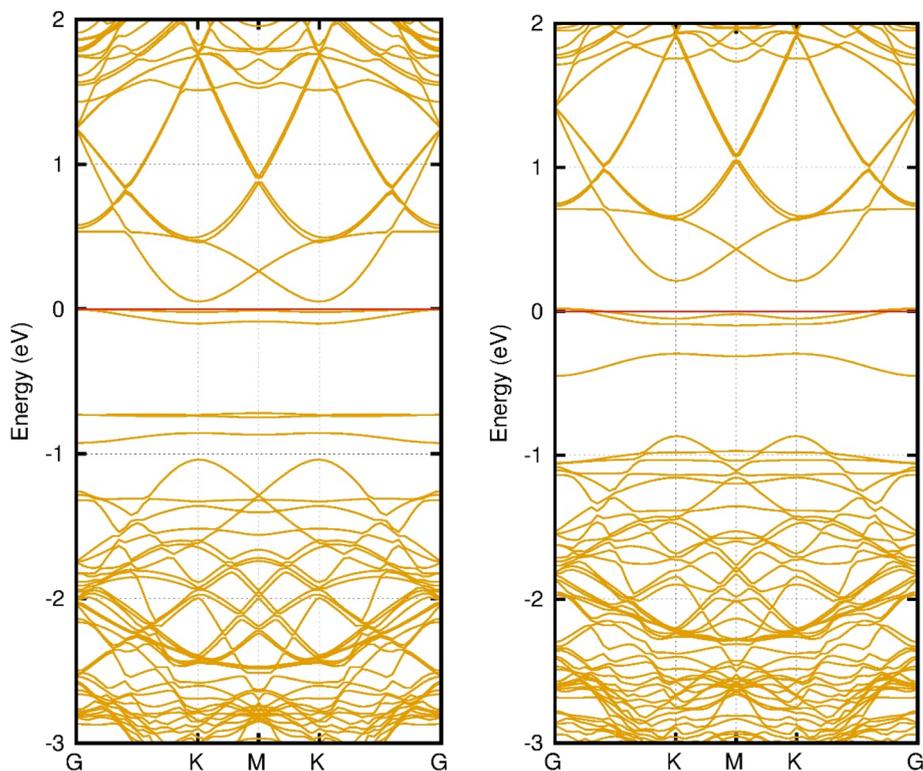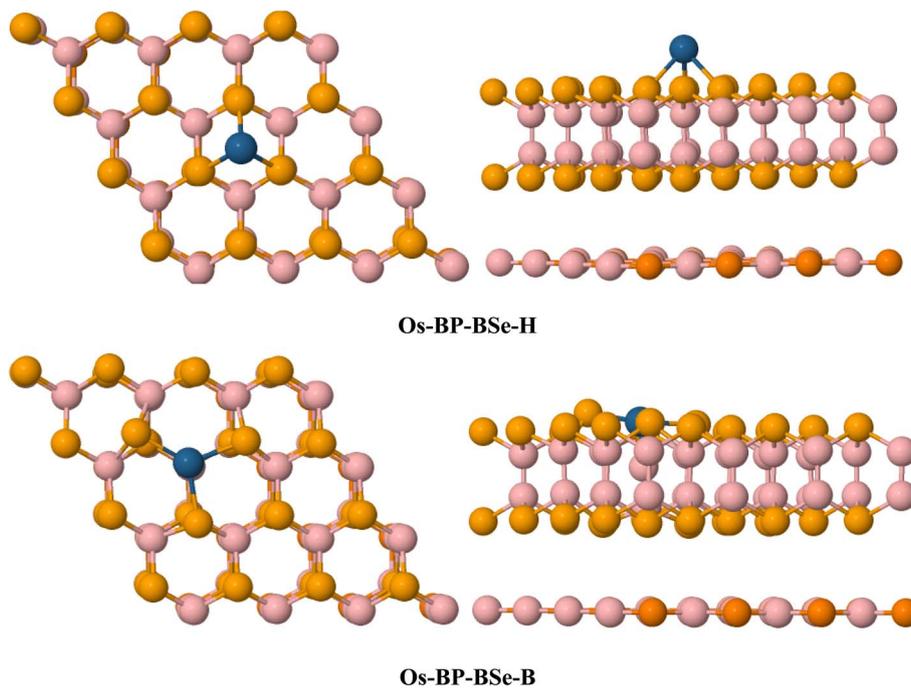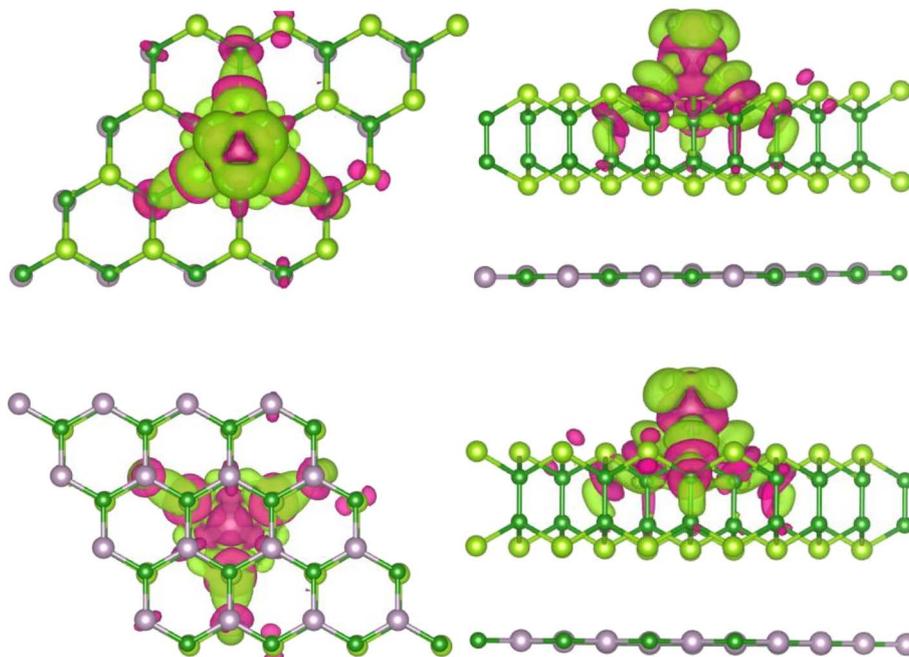
the pristine BP/BSe heterostructure was initially optimized to provide an appropriate material for doping with Ir and Os atoms. Fig. 1(a–c) displays the heterostructure system composed of BP and BSe monolayers, which are vertically aligned with each other. The B and P atoms of the BP monolayer were relaxed over the Se and B atoms of the BSe monolayer. The band structure plot of the BP/BSe heterostructure is displayed in Fig. 1(d). Similar to the intrinsic BP and BSe monolayers, the

constructed BP/BSe heterostructure also shows semiconductor properties with a band gap of about 1.20 eV, revealing the tunable electronic characteristics of the pristine heterostructure.

Subsequently, Ir and Os atoms were adsorbed on the BSe monolayer surface to modify the original BP/BSe heterostructures for efficient adsorption of gas molecules. Two different sites for Ir and Os adsorption were analyzed including the H and B sites, which display the binding of the transition metal to the top of a hollow site and the top of a B site, respectively. The optimized structures of Ir modified BP/BSe heterostructures at different binding sites are shown in Fig. 2. As shown in the first modified heterostructure, the Ir atom is adsorbed on the hollow site of the BSe system and forms three chemical bonds with three neighboring Se atoms. In the second modified system, the Ir atom is adsorbed at the top of the B site and also forms three covalent bonds with the adjacent Se atoms. Table 1 summarizes the relevant energy and geometrical parameters. As shown in Table 1, the final Ir–Se bond lengths for binding of Ir atoms on the BP/BSe heterostructure are 2.51 Å and 2.48 Å, respectively.

The formation energies were calculated to demonstrate the structural stability of the Ir and Os doped BP/BSe heterostructures. The formation energy is calculated using the following equation:

$$E_{form} = E_{(BP/BSe@M)} - E_{(BP/BSe)} - E_{(M)} \qquad (2)$$

where $E_{(BP/BSe@M)}$, $E_{(BP/BSe)}$ and $E_{(M)}$ represent the energies of the Ir or Os modified BP/BSe heterostructure, bare BP/BSe heterostructure and Ir or Os atoms, respectively. Our results showed that the formation energies of Ir doping on the top of H and B sites are −3.17 eV and −2.80 eV, respectively, both verifying the stable heterostructure formation by Ir modification.

To further elucidate the interaction between the heterostructures and transition metals, we examined the electronic properties of Ir and Os modified BP/BSe heterostructure systems, including the band structure (BS) and charge density difference (CDD). Fig. 3 and 4 display the CDD profiles of the Ir modified BP/BSe heterostructure systems. The violet and green colors signify charge accumulation and depletion, respectively. The CDDs provide valuable insights into the bonding characteristics between Ir/Os atoms and the Se atoms of the BSe system. Evidently, substantial charge accumulation is observed near the Ir atom and the neighboring Se atoms, whereas charge depletion mainly happens away from the Ir atom. This considerable charge accumulation verifies the strong covalent interaction between Ir and Se atoms.

The electronic band structure of the Ir modified BP/BSe heterostructure is also displayed in Fig. 5. After adsorption of Ir at the BSe site of the BP/BSe heterostructure, the modified systems exhibit semiconducting characteristics, and the conductivity is enhanced due to band gap diminution.

Next, we studied the optimized structures and properties of Os modified BP/BSe heterostructures, as depicted in Fig. 6. The calculated formation energies for Os doping on the top of H
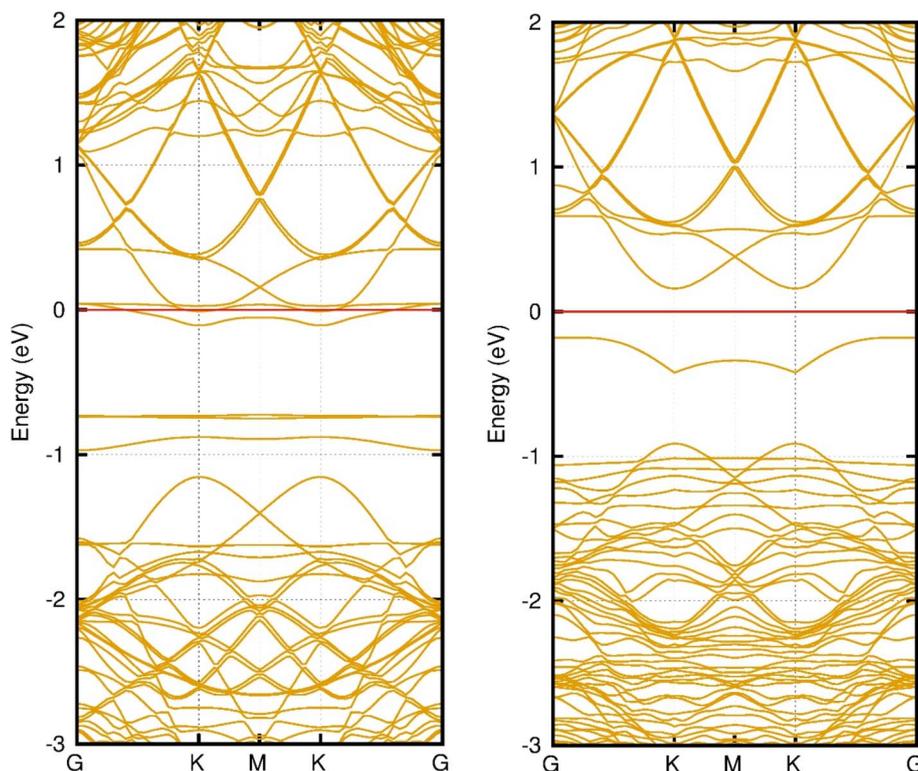

Fig. 8 Band structure diagrams of the Os modified BP/BSe heterostructure systems.

and B sites of the BP/BSe heterostructure are −1.92 eV and −1.76 eV, respectively. Thus, the Os doped BP/BSe heterostructures are structurally stable with Os–Se bond lengths of 2.46 Å and 2.39 Å.

The results suggest that Ir doping on the BP/BSe heterostructure leads to a higher formation energy than Os doping on the considered heterostructure. Thus, Ir-BP/BSe heterostructures have higher stability than the Os-BP/BSe ones, implying their suitability for adsorbing H_2S, SO_2F_2 and SOF_4 gas molecules. The charge accumulation between the Os and Se atoms based on CDD diagrams (Fig. 7) illustrates a noticeable chemical reaction between these atoms. The band structures of the Os modified BP/BSe heterostructures are also displayed in Fig. 8, indicating that the semiconducting property of the Os modified system remains unchanged. By analyzing the formation energies and CDD results, we conclude that the Ir and Os atoms strongly interact with the BP/BSe heterostructures.

3.2 Adsorption of H_2S, SO_2F_2 and SOF_4 gas molecules on Ir-BP/BSe heterostructures

Ir modified BP/BSe heterostructures were examined for their high adsorption capacity towards H_2S, SO_2F_2 and SOF_4 gas molecules. Fig. 9 displays the optimized Ir-BP/BSe heterostructures with adsorbed H_2S and SO_2F_2 molecules, and they are labeled as Ir-BP–BSe@H_2S and Ir-BP–BSe@SO_2F_2. H_2S molecules are adsorbed on the Ir site of the heterostructure *via* the central S atom, achieving an adsorption energy of −0.68 eV and 2.33 Å distance between the Ir and S atoms.

For SO_2F_2 adsorption, there are two ways; one in which the F atoms of the molecule are close to the Ir site of the modified heterostructure and another in which the O atoms are near the Ir site, as shown in Fig. 9. In the case of F atoms near the Ir site, the cleavage of S–F bonds occurs after the adsorption of SO_2F_2 on the Ir-BP–BSe heterostructure. The adsorption energy for the SO_2F_2 molecule on the Ir-BP–BSe heterostructure is −2.97 eV, which is large to support such
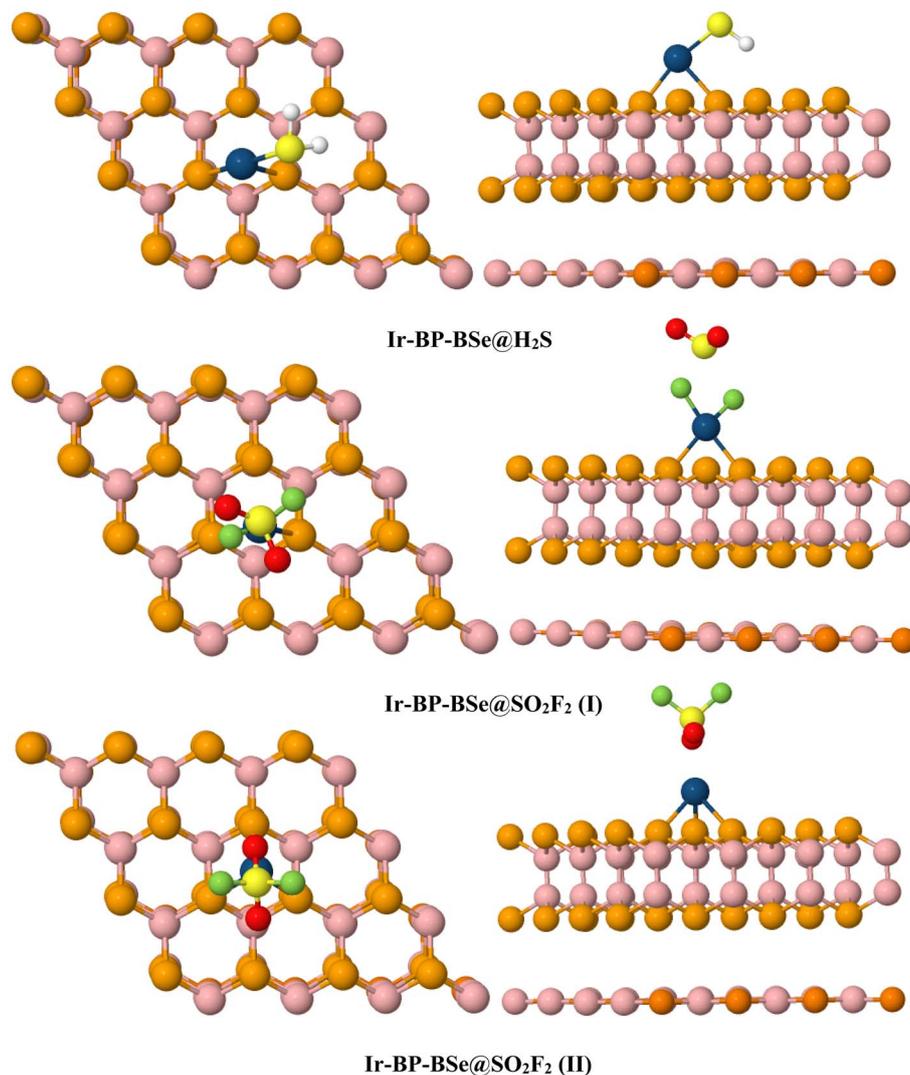

Ir-BP-BSe@H₂S

Ir-BP-BSe@SO₂F₂ (I)

Ir-BP-BSe@SO₂F₂ (II)

Fig. 9 Optimized configurations of the Ir modified BP/BSe heterostructure systems with adsorbed H_2S and SO_2F_2 gas molecules.
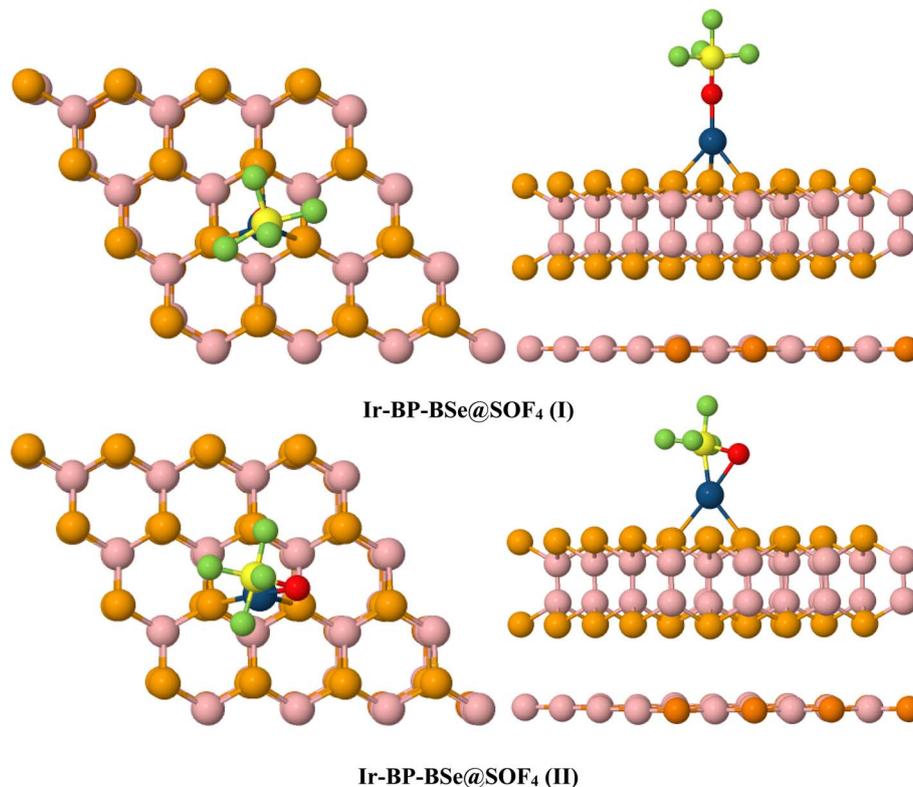
Ir-BP-BSe@SOF₄ (I)

Ir-BP-BSe@SOF₄ (II)

Fig. 10 Optimized configurations of the Ir modified BP/BSe heterostructure systems with adsorbed SO_2F_2 and SOF_4 gas molecules.

a dissociative reaction, while the adsorption of SO_2F_2 through the O atoms exhibits a small adsorption energy of -0.45 eV. For the Ir-BP–BSe@SO_2F_2 heterostructure, the adsorption distances are 1.98 Å and 2.78 Å for the Ir–F and Ir–S bonds, respectively. SOF_4 adsorption systems on the Ir modified BP--BSe heterostructures are depicted in Fig. 10. The considerable adsorption energies of -2.55 eV and -2.62 eV indicate strong chemical adsorption of SOF_4 on the substrates. The SOF_4 adsorption distance between the Ir and O atoms is 2.07 Å, which is short enough to confirm such a strong interaction. Hence, the results show that doping BP/BSe heterostructures with Ir atom increases the adsorption energy and decreases the adsorption distance for gas molecules. Fig. 11 displays the electronic properties based on the band structures for the Ir modified BP/BSe heterostructures with adsorbed H_2S, SO_2F_2 and SOF_4 gas molecules. This figure reveals remarkable variations in the band structure plots upon adsorption of H_2S, SO_2F_2 and SOF_4 molecules. However, the semiconducting feature is obviously retained even after interaction with the gas molecules. The CDDs were evaluated to examine the chemical adsorption of gases on the Ir-BP–BSe heterostructures (Fig. 12). As can be seen, the concentration of charge density is primarily observed over the adsorbed H_2S, SO_2F_2 and SOF_4 gas molecules. Ir doping of BP–BSe heterostructures, as well as the adsorption of SO_2F_2 and SOF_4 molecules, introduce new changes in their PDOS, as

illustrated by the relevant diagrams in Fig. 13. These changes are attributed to the noticeable overlaps between the Ir and O atoms and the resulting remarkable hybridization between the d orbital of Ir and the p orbital of the O atom in the SOF_4 adsorption system. Besides, the PDOS peaks of the S and F atoms of SO_2F_2 molecules are separated from each other, indicating the S–F bond cleavage.

3.3 Sensitivity of the novel Ir-BP–BSe heterostructure

Substantial changes in the work function (Φ) can create an electrical signal, which is mainly utilized for detecting and sensing target molecules.[39,40] Thus, the potential application of the novel Ir modified BP–BSe heterostructure as Φ-type sensors is investigated here. The work function variations are analyzed using the following equation:

$$\Phi = V_{(\Phi)} - E_{\text{f}} \tag{3}$$

where $V_{(\Phi)}$ stands for the electrostatic potential of the vacuum level and E_{f} represents the energy of the Fermi level. The work function of the pristine BP–BSe heterostructure is 5.25 eV, which increases or decreases after gas molecule adsorption on the surface. The changes in Φ before and after interaction with gas molecules are shown in Table 2, where negative and positive values denote a decrease and an increase in the work function after detecting gas molecules. The SO_2F_2 adsorption system in
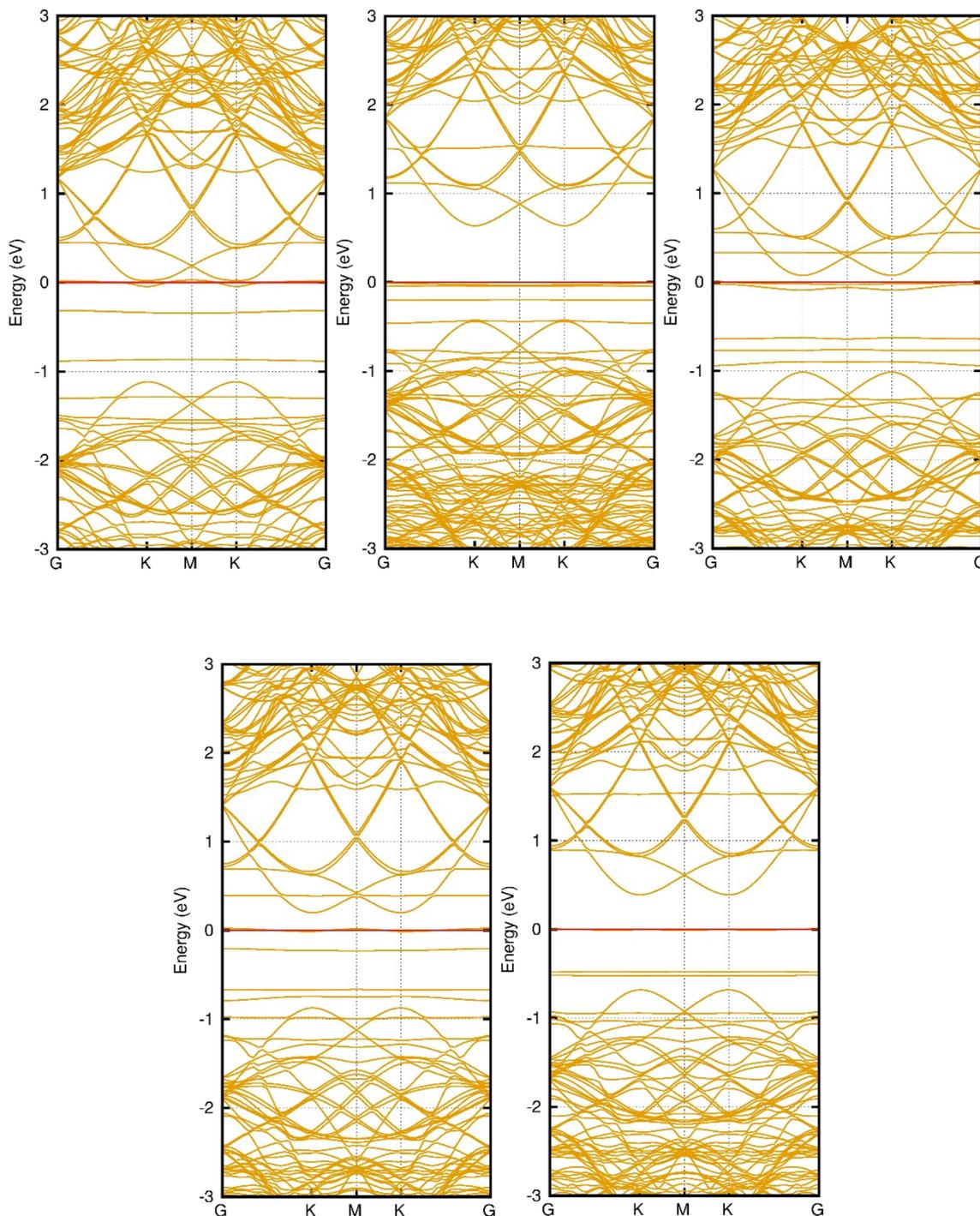
Fig. 11 Band structure diagrams of the Ir modified BP/BSe heterostructure systems with adsorbed H$_2$S, SO$_2$F$_2$ and SOF$_4$ gas molecules.

the second configuration exhibits the highest work function change, which can be ascribed to its highest adsorption energy. For SOF$_4$ adsorption configurations, positive changes of 0.38 eV and 0.67 eV are observed, indicating that the work function of the BP–BSe heterostructure increases after SOF$_4$ adsorption. These results highlight the unique potential of Ir modified BP–BSe heterostructures as suitable sensors for detecting H$_2$S, SO$_2$F$_2$ and SOF$_4$ gas molecules.

3.4 Recovery time

Due to the substantial importance of quick desorption of gas molecules from the surface of sensor, short recovery time plays a crucial role in the efficient functioning of sensor devices. It is worth mentioning that very strong adsorption of gas molecules on the substrates gives rise to the higher adsorption energies and thus prolonged recovery times. In addition, long recovery
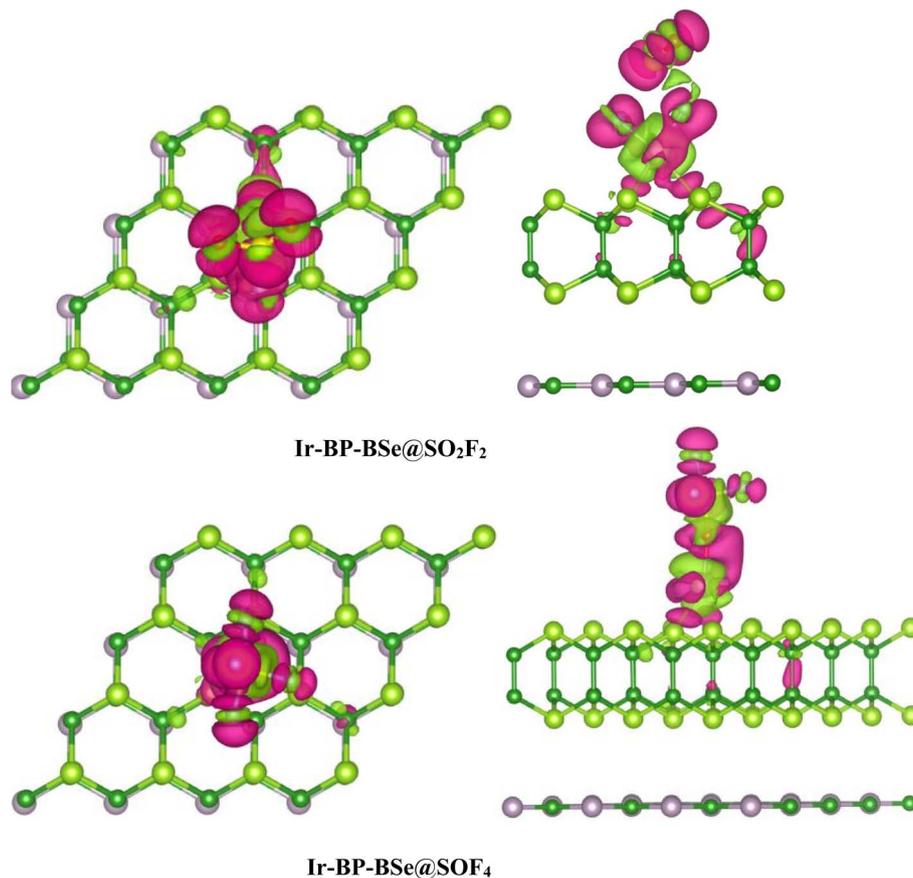
Ir-BP-BSe@SO₂F₂

Ir-BP-BSe@SOF₄

Fig. 12 CDD diagrams of the Ir modified BP/BSe heterostructure systems with adsorbed SO_2F_2 and SOF_4 gas molecules.
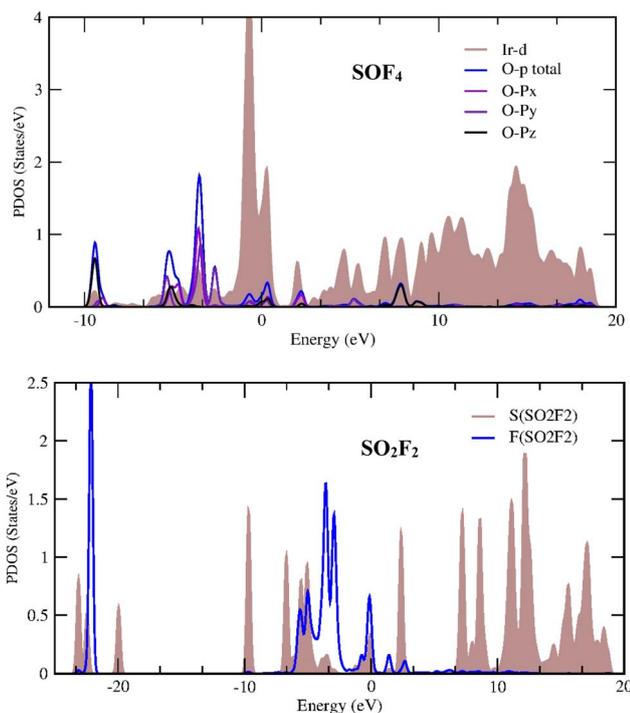

Fig. 13 Projected DOS diagrams of the Ir modified BP/BSe heterostructure systems with adsorbed SO_2F_2 and SOF_4 gas molecules.

times are not ideal for electronic gas sensors. Therefore, the recovery times were determined for the desorption of the considered gases from the surface of the Ir modified BP–BSe heterostructure and listed in Table 2. The recovery times of gas molecules on the Ir modified BP–BSe heterostructure are calculated using eqn (4):

$$\tau = v_o^{-1}\exp\left(\frac{-E_{ads}}{K_B\,T}\right) \qquad (4)$$

where E_{ads} is the adsorption energy, k_B is Boltzmann's constant and T denotes the temperature. Based on the abovementioned equation, more negative adsorption energies can lead to longer recovery times. The recovery times at 298 K for the most stable adsorption configurations of the H_2S, SO_2F_2 and SOF_4 molecules on the Ir modified BP–BSe heterostructures are calculated to be 0.32 s, 1.60×10^{38} s, and 1.98×10^{32} s, respectively (see Table 2). Thus, the Ir modified BP–BSe heterostructure exhibits a much longer recovery time for SO_2F_2 and SOF_4 molecules, while the recovery time for H_2S desorption is short, implying that H_2S sensing is more suitable based on the Ir modified BP–BSe heterostructure. Additionally, according to eqn (4), when the temperature increases during the adsorption of gases, the recovery time decreases.

Table 2 Adsorption results like adsorption energies (E_{ad}), distances (d), work functions (Φ), work function changes ($\Delta\Phi$) and recovery times (τ) for SO_2, SO_2F_2 and SOF_4 molecules on the Ir modified BP/BSe heterostructures

Structure	E_{ad} (eV)	d (Å)	Φ (eV)	$\Delta\varphi$ (eV)	τ (s)
Ir-BP-BSe@H2S	−0.68	2.33 (Ir–S)	5.00	−0.25	0.32
Ir-BP-BSe@SO2F2(ɪ)	−2.97	1.98 (Ir–F)	6.25	1.00	1.60×10^{38}
Ir-BP-BSe@SO2F2(ɪɪ)	−0.45	2.78 (Ir–S)	5.21	−0.04	4.06×10^{-5}
Ir-BP-BSe@SOF4(ɪ)	−2.55	2.07 (Ir–O)	5.63	0.38	1.33×10^{31}
Ir-BP-BSe@SOF4(ɪɪ)	−2.62	2.16 (Ir–O), 2.31 (Ir–S)	5.92	0.67	1.98×10^{32}

4. Conclusions

Using density functional theory calculations, this work explores the structures and electronic properties of Ir and Os modified BP/BSe heterostructures and examines the adsorption and sensing properties of these novel systems towards H_2S, SO_2F_2 and SOF_4 gas molecules. The strong binding of Ir and Os atoms to the BSe side of the heterostructures through chemical bonds is further verified by charge accumulation in the interfacial region. The structural stability of Ir- and Os-BP/BSe heterostructures is demonstrated by formation energy calculations. Among the considered H_2S, SO_2F_2 and SOF_4 gas molecules, SO_2F_2 molecules exhibit the highest adsorption energy with strong chemisorption and cleavage of S–F bonds. The work functions, density of states and recovery times were also analyzed to further explore the adsorption process based on novel heterostructures. This work indicates that Ir and Os binding can improve the adsorption of molecules on the surface of BP/BSe heterostructures. Accordingly, Ir- and Os-BP/BSe heterostructures emerge as excellent nanomaterials for gas adsorption, providing a theoretical basis for the development of highly effective gas sensors.

Data availability

Data will be available on reasonable request to the corresponding Author (Prof. Amirali Abbasi).

Conflicts of interest

There are no conflicts to declare.

References

1 A. Abbasi and J. Jahanbin Sardroodi, Structural and electronic properties of group-IV tin nanotubes and their effects on the adsorption of SO_2 molecules: insights from DFT computations, *J. Appl. Phys.*, 2018, **124**, 165302.

2 B.-W. Zhang, D. Fang, X. Fang, H.-B. Zhao, D.-K. Wang, J.-H. Li, X.-H. Wang and D.-B. Wang, InAs/InAsSb type-II superlattice with near room-temperature long-wave emission through interface engineering, *Rare Met*, 2022, **41**, 982–991.

3 X. Liu, S. Cheng, H. Liu, S. Hu, D. Zhang and H. Ning, A survey on gas sensing technology, *Sensors (Basel)*, 2012, **12**, 9635–9665.

4 A. Abbasi and J. J. Sardroodi, An innovative gas sensor system designed from a sensitive nanostructured ZnO for the selective detection of SO_x molecules: a density functional theory study, *New J. Chem.*, 2017, **41**, 12569–12580.

5 A. Abbasi and J. J. Sardroodi, Investigation of the adsorption of ozone molecules on TiO_2/WSe_2 nanocomposites by DFT computations: applications to gas sensor devices, *Appl. Surf. Sci.*, 2018, **436**, 27–41.

6 Z. Nie, C. Wang, R. Xue, G. Xie and H. Xiong, Two-dimensional FePc and MnPc monolayers as promising materials for SF_6 decomposition gases detection: Insights from DFT calculations, *Appl. Surf. Sci.*, 2023, **608**, 155119.

7 R. Xue, Y. Guo, H. He, Y. Zhang, N. Yang, G. Xie and Z. Nie, Bimetallic phthalocyanine monolayers as promising materials for toxic H_2S, SO_2, and SOF_2 gas detection: insights from DFT calculations, *Langmuir*, 2025, **41**(6), 4059–4075.

8 Z. Nie, R. Xue, X. He, G. Xie and H. Xiong, Atomic regulation to improve the sensing-performance of CoPc and NiPc monolayer toward chloromethane molecule: insights from DFT calculations, *Surf. Interfaces*, 2023, **43**, 103542.

9 G.-X. Chen, R.-Y. Du, D.-D. Wang, Z. Chen, S. Liu and J.-M. Zhang, Adsorption of NO gas molecule on the vacancy defected and transition metal doped antimonene: a first-principles study, *Vacuum*, 2023, **207**, 111654.

10 J. He, G. Liu, C. Zhang and G. Zhang, First-principles study of non-metallic edge-modified zigzag arsenene nanoribbons for CO adsorption, *Chin. J. Phys.*, 2023, **83**, 628–636.

11 Y. Wang, Y. Zheng, J. Xiao, L. Xu, X. Dai and Z. Wang, Effect of transition metal modification on the sensing characteristics of arsenene adsorption of nitrogenous toxic gases, *Vacuum*, 2023, **210**, 111845.

12 S. G. Chatterjee, S. Chatterjee, A. K. Ray, *et al.*, Graphene–metal oxide nanohybrids for toxic gas sensor: a review, *Sens. Actuators, B Chem.*, 2015, **221**, 1170–1181.

13 S. W. Lee, W. Lee, Y. Hong, *et al.*, Recent advances in carbon material-based NO_2 gas sensors, *Sens. Actuators, B*, 2018, **255**, 1788–1804.

14 Z. Xiao, L. B. Kong, S. Ruan, *et al.*, Recent development in nanocarbon materials for gas sensor applications, *Sens. Actuators, B*, 2018, **274**, 235–267.

15 W. Shao, C. He, M. I. Zhou, *et al.*, Core-shell-structured MOF-derived 2D hierarchical nanocatalysts with enhanced Fenton-like activities, *J. Mater. Chem. A*, 2020, **8**, 3168–3179.

16 N. Hakimi Raad, N. Manavizadeh, I. Frank and E. Nadimi, Gas sensing properties of a two-dimensional graphene/h-BN multi-heterostructure toward H_2O, NH_3 and NO_2: a first principles study, *Appl. Surf. Sci.*, 2021, **565**, 150454.

17 S. Ma, L. Su, L. Jin, J. Su and Y. Jin, A first-principles insight into Pd-doped $MoSe_2$ monolayer: a toxic gas scavenger, *Phys. Lett.*, 2019, **383**, 125868.

18 J. Ren, Y. Xue and L. Wang, SO_2 gas adsorption on the transition metal (Pd, Ag, Au and Pt)-doped monolayer $MoSe_2$: a first-principles study, *Chem. Phys. Lett.*, 2020, **747**, 137380.

19 S. Kaviani, I. I. Piyanzina, O. V. Nedopekin and D. A. Tayurskii, Adsorption behavior and sensing properties of toxic gas molecules onto Pt_nBe ($n = 5, 7, 10$) clusters: a DFT benchmark study, *Mater. Today Commun.*, 2022, **33**, 104851.

20 C. X. Xia, J. Du, X. W. Huang, W. B. Xiao, W. Q. Xiong, T. X. Wang, *et al.*, Two-dimensional *n*-InSe/p-GeSe(SnS) van der Waals heterojunctions: high carrier mobility and broad band performance, *Phys. Rev. B*, 2018, **97**, 115416.

21 D. H. Wang, W. W. Ju, D. W. Kang, T. W. Li and H. S. Li, Tunable electronic, optical, and spintronic properties in $InSe/MTe_2$ (M =Pd, Pt) van der Waals heterostructures, *Vacuum*, 2021, **183**, 109859.

22 M. Yankowitz, Q. Ma, P. Jarillo-Herrero, *et al.*, van der Waals heterostructures combining graphene and hexagonal boron nitride, *Nat. Rev. Phys.*, 2019, **1**, 112–125.

23 Y. Liu, N. O. Weiss, X. Duan, *et al.*, Van der Waals heterostructures and devices, *Nat. Rev. Mater.*, 2016, **1**, 16042.

24 D. Jariwala, T. J. Marks and M. C. Hersam, Mixed-dimensional van der Waals heterostructures, *Nat. Mater.*, 2017, **16**, 170–181.

25 W. Zheng, X. Liu, J. Xie, *et al.*, Emerging van der Waals junctions based on TMDs materials for advanced gas sensors, *Coord. Chem. Rev.*, 2021, **447**, 214151.

26 X. Meng, Y. Shen, J. Liu, *et al.*, The $PtSe_2$/GaN van der Waals heterostructure photocatalyst with type II alignment: a first-principles study, *Appl. Catal., A*, 2021, **624**, 118332.

27 G. Guo, S. Luo, C. Lai, *et al.*, Substitutional doping effect of C3N anode material: a first principles calculations study, *Appl. Surf. Sci.*, 2022, **571**, 151330.

28 A. Abbasi, R. M. Rzayev, A. A. Niyazova, D. Sur, S. Ballal, N. K. Karimova and A. E. Suleymanova, Enhanced adsorption and biosensing performance of adenine ($C_5H_5N_5$) and Guanine ($C_5H_5N_5O$) nucleobases on the novel $ZnO-MoSe_2$ nanosheets: a theoretical study, *Mater. Chem. Phys.*, 2025, **337**, 130559.

29 Y. Zhang, W. Feng, J. Zhang, *et al.*, Enhancement of adsorption performance of gases in oil on a Cr_3-modified SnS_2 monolayer based on the first principles, *Langmuir*, 2023, **39**, 14422–14432.

30 A. Abbasi, Tuning the structural and electronic properties and chemical activities of stanene monolayers by embedding 4d Pd: a DFT study, *RSC Adv.*, 2019, **9**, 16069–16082.

31 Y. Bo, Q. Zhang, X. Yang, B. Wang and Y. Shen, Detection of harmful gases (NO, NO_2) by GaN@MoSSe heterostructures embedded with transition metal (Cu, Fe and Mn) atoms: a DFT study, *Surf. Interfaces*, 2024, **54**, 105151.

32 P. Hohenberg and W. Kohn, *Phys. Rev.*, 1964, **136**, B864–B871.

33 W. Kohn and L. Sham, *Phys. Rev.*, 1965, **140**, A1133–A1138.

34 J. M. Soler, E. Artacho, J. D. Gale, A. Garca, J. Junquera, P. Ordejn and D. Snchez-Portal, The SIESTA method for *ab initio* order-N materials simulation, *J. Phys. Condens. Matter.*, 2002, **14**, 2745–2779.

35 J. P. Perdew, K. Burke and M. Ernzerhof, *Phys. Rev. Lett.*, 1997, **78**, 1396.

36 A. Koklj, Computer graphics and graphical user interfaces as tools in simulations of matter at the atomic scale, *Comput. Mater. Sci.*, 2003, **28**, 155–168.

37 H. J. Monkhorst and J. D. Pack, Special points for Brillouin-zone integrations, *Phys. Rev. B: Condens. Matter Mater. Phys.*, 1976, **13**, 5188–5192.

38 S. Grimme, J. Antony, S. Ehrlich and H. A. Krieg, consistent and accurate *ab initio* parametrization of density functional dispersion correction (DFT-D) for the 94 elements H-Pu, *J. Chem. Phys.*, 2010, **132**, 154104.

39 F. Li, X. Gao, R. Wang, T. Zhang and G. Lu, Study on TiO_2-SnO_2 core-shell heterostructure nanofibers with different work function and its application in gas sensor, *Sens. Actuators, B*, 2017, **248**, 812–819.

40 P. Shanmugam, R. Kalidoss, A. Sundaramurthy and Y. Sivalingam, Work function analysis of photoenhanced triethylamine adsorption impact on Au embedded CeO_2 coated ZnO hybrid nanostructures: an investigation by scanning kelvin probe, *Surf. Interfaces*, 2024, **44**, 103749.